PERGAMON

International Journal of Solids and Structures 38 (2001) 4177–4198

INTERNATIONAL JOURNAL OF SOLIDS and STRUCTURES

www.elsevier.com/locate/ijsolstr

Modeling of reinforced masonry elements

Sonia Marfia, Elio Sacco *

Dipartimento di Meccanica Strutture Ambiente e Territorio, Università di Cassino Via di G. di Biasio 43, 03043 Cassino, Italy

Received 19 June 2000

Abstract

In this paper, a micromechanical investigation for the evaluation of the overall response of the masonry material reinforced by innovative composite materials is developed. The masonry is regarded as a heterogeneous medium realized by a regular arrangement of blocks into a matrix of mortar. A homogenization procedure is developed for a one-dimensional reinforced masonry problem, considering the progressive damage and plasticity of the mortar and the block. Moreover, the brittle failure of the fiber reinforced plastic reinforcement is accounted for. The delamination effect of the composite sheets from the masonry element is also modeled. A numerical procedure, based on the arc-length method with a backward-Euler integration of the evolutive equations, is developed to study the behavior of the reinforced masonry. Numerical applications regarding the axial and the bending response of the material are presented.

Keywords: Reinforced masonry; Damage; Plasticity; Homogenization

1. Introduction

Masonry structures represent the largest part of the construction heritage in the world. In fact, monuments and historic buildings and also many houses, bridges and simple constructions are realized in masonry material.

From a structural viewpoint, the masonry material is characterized by a very low tensile strength; thus, even reduced values of the tensile stresses can induce crack initiation and hence damage of the material. Because of the limited tensile strength, masonry constructions often present diffuse fracture patterns. Moreover, masonry bearing and shear walls have been found to be vulnerable to earthquakes.

The ability to perform satisfactory stress analyses of masonry structures and to design appropriate reinforcements has been and is, even nowadays, an important problem for engineers. The stress analyses should provide information about the safety of the structure; in fact, the presence of fractures in a masonry structure can be pathological or physiological, and hence it could or could not require strengthening. On the other hand, because of the difficulty in performing accurate stress analyses, technicians often prefer to reinforce masonry structures even when it is not strictly necessary.

* Corresponding author. Fax: +390-776-310-812.
E-mail address: sacco@ing.unicas.it (E. Sacco).

0020-7683/01/$ - see front matter
PII: S0020-7683(00)00297-3

Two different approaches have been developed in the literature in order to analyze the behavior of masonry structures: the discrete and the continuous models. The first kind of models are used to study monumental structures made of big superimposed blocks. Within these models, the blocks are usually schematized as linear elastic while the behavior of the interfaces is modeled by the unilateral Coulomb friction law (Yim et al., 1990; Grimaldi et al., 1992). On the other hand, several continuous models have been proposed for the masonry, based either on phenomenological or on micromechanical laws. As an example, the 'no-tension' model considers the masonry as a homogeneous elastic material which cannot support tensile stresses (Heyman, 1966; Giaquinta and Giusti, 1985; Romano and Sacco, 1987). The micromechanical approach allows one to derive the masonry response, modeling the masonry as a heterogeneous material, often with periodic microstructure, realized by bricks in a matrix of mortar (Pande et al., 1989; Kralj et al., 1991; Pietruszczak and Niu, 1992; Anthoine, 1995; Luciano and Sacco, 1995, 1997; Gambarotta and Lagomarsino, 1997a,b).

From a technological point of view, the strengthening of masonry structures has been accomplished adopting standard materials, mainly cement, concrete and steel, sometimes with the aim of changing the statics of the structure. Simplified stress analyses and strengthening procedures are suggested in specialized literature. In the past, new reinforcement approaches are rising; they are based on the idea that the strengthening should be light and removable and, if possible, it should not change the structural scheme of the construction.

Composite materials appear to be good candidates to substitute standard materials, since they are light, very simple to install and are also removable. Moreover, composite materials are characterized by high strength, good resistance to corrosion, durability and reduced installation and maintenance costs. As a matter of fact, composite materials have been successfully used in several fields of structural civil engineering (Neale and Labossière, 1992; El-Badry, 1996), mainly for strengthening concrete and wood structures (Nanni, 1993; Meier, 1987).

Thus, one promising technique to improve the overall strength of masonry structures and to reduce their seismic vulnerability is to retrofit the masonry walls using fiber reinforced plastic (FRP). This system consists of glass, carbon or aramidic fiber fabric combined with special epoxies to create a high strength, lightweight structural laminate. FRP reinforcements can be designed to work in conjunction with existing walls to increase both the in-plane and out-of-plane strength of the unreinforced masonry walls. Triantafillou and Fardis (1993, 1995) and Triantafillou (1996) studied the applications of advanced composites for strengthening historical masonry structures. The behavior of walls, reinforced by carbon fiber sheets or conventional woven fabric bonded on the masonry surfaces, have been investigated with experimental tests by Schwegler (1994). Luciano and Sacco (1996, 1998) proposed a simple model for studying the behavior of masonry panels reinforced by FRP sheets.

Recently, applications of advanced composites are successfully adopted to restore masonry structures. In particular, several masonry structures damaged by the last earthquake in Umbria (Italy) have been reinforced using composite materials. This fact emphasizes the increasing interest in the use of FRP for the reinforcement of existing masonry, and the need to develop satisfactory structural analyses. It can be pointed out that appropriate models and computational procedure able to predict the response of reinforced masonry are lacking.

In order to fill the gap between the technological interest and the development of appropriate design suggestions, this paper is aimed at investigating the overall behavior of the masonry reinforced by means of FRP composite materials. In particular, a one-dimensional micromechanical analysis is developed to evaluate the overall mechanical response, adopting a nonlinear homogenization technique.

Although one-dimensional beam models could appear too simple and may be limited, they allow us to study the behavior of several masonry structural elements. In fact, arcs and architraves are typical examples of one-dimensional elements. On the other hand, beam models can be successfully used to study the out-of-plane bending behavior of masonry walls or the response of vaults reinforced by circumferential chains.

The model proposed in this paper accounts for damage in tension and damage and plasticity in compression for the block and the mortar. The reinforcement brittle failure is also considered. Moreover, the delamination process of the FRP from the masonry is studied by means of the Griffith energetic criterion. Furthermore, a numerical procedure, based on the arc-length technique with an appropriate choice of the control parameters, is developed. Some numerical applications regarding the study of the axial and the bending response of the reinforced masonry under different loading histories are presented. The beneficial effect of FRP reinforcement on the masonry behavior is emphasized.

The paper is organized as follows: first, the reinforced masonry model is proposed, introducing the damage-plastic constitutive laws for the block and the mortar. Moreover, the brittle behavior of the FRP is taken into account and an evolutive criterion for the delamination is considered. Then, the numerical procedure and the proposed algorithm are described. Finally, some numerical results are presented.

2. Masonry and reinforcement modeling

In order to study the behavior of the reinforced masonry, a micromechanical analysis is performed. The aim of this approach is to investigate the effects of the damage of different components of the reinforced masonry, on the overall response of the material. In fact, the behavior of the masonry is influenced by the damage of the mortar, the damage of the blocks, the delamination of the composite from the masonry and the failure of the reinforcement.

In the masonry arrangement, vertical and horizontal thin layers of mortar are present. Because of the reduced thickness, the mortar can be modeled in the masonry by a continuous as well as by a special interface material joining the blocks.

The attention is focussed on the study of a one-dimensional masonry element, as shown in Fig. 1. It consists in a beam obtained as a repetitive sequence of blocks and mortar. Moreover, FRP sheets are partially glued on the top and bottom of the beam. In Fig. 2, the unit cell representing one-half of the repetitive microstructure is reported; the total length of the unit cell is $L = L_b + L_m$, where L_b and L_m denote the block and mortar halflengths.

The reinforced masonry can be regarded as obtained superimposing two different elements: the masonry and the reinforcement. The first one has constant rectangular cross-section $A_M = b \times h$. The second one is defined by the reinforcements on the top and the bottom of the masonry, which are characterized by the areas A_R^+ and A_R^-, respectively. With reference to Fig. 2, it is assumed that the reinforcement is in perfect adhesion on the block for a length equal to L_g and it is completely unglued in the zone corresponding to the mortar, characterized by the length $L_u = L - L_g$.

With the aim of deriving the overall response for the defined unit cell in terms of resultant axial force and bending moment as function of the average axial strain and curvature, one-dimensional continuous stress–strain relations for the mortar and the block are introduced and a FRP damage mechanism is considered.

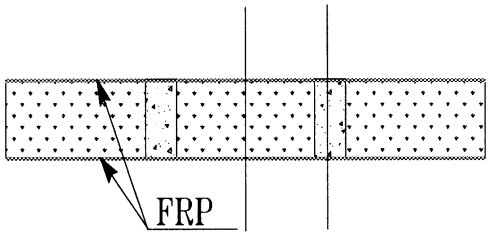

Fig. 1. Heterogeneous reinforced masonry beam.

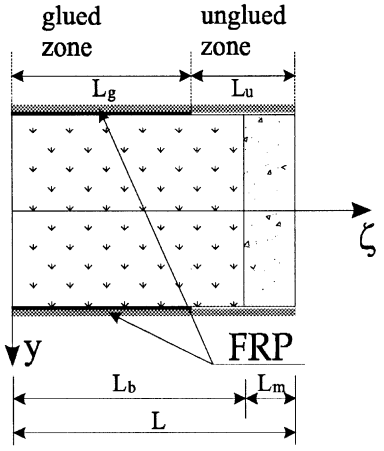

Fig. 2. Unit cell obtained from the periodicity and symmetry of the masonry.

2.1. Mortar and block

A simple one-dimensional constitutive relation is chosen both for the mortar and the block. It is characterized by a damage response in traction and damage-plasticity law in compression. In particular, the constitutive equation is (Lemaitre and Chaboche, 1990)

$$\sigma = (1 - D)E(\varepsilon - \varepsilon_{\mathrm{p}}), \tag{1}$$

where D is the damage parameter and ε_{p} is the plastic strain, so that $\varepsilon - \varepsilon_{\mathrm{p}} = \varepsilon_{\mathrm{e}}$ represents the elastic strain. The Young's modulus E of the block and mortar are denoted as E_{b} and E_{m}, respectively.

2.1.1. Damage

A damage evolution law, inducing a linear softening in the stress–strain relationship, is assumed:

$$0 \leqslant \dot{D} = \begin{cases} 0 & \text{for } \varepsilon_{\mathrm{d}} < \varepsilon_{\mathrm{c}}^{\pm}, \\ \dfrac{\varepsilon_{\mathrm{c}}^{\pm}\varepsilon_{\mathrm{u}}^{\pm}}{\left(\varepsilon_{\mathrm{u}}^{\pm} - \varepsilon_{\mathrm{c}}^{\pm}\right)\varepsilon_{\mathrm{d}}^{2}}\dot{\varepsilon} & \text{for } \varepsilon_{\mathrm{c}}^{\pm} < \varepsilon_{\mathrm{d}} < \varepsilon_{\mathrm{u}}^{\pm}, \\ 0 & \text{for } \varepsilon_{\mathrm{u}}^{\pm} < \varepsilon_{\mathrm{d}}, \end{cases} \tag{2}$$

where $\varepsilon_{\mathrm{c}}^{\pm}$ and $\varepsilon_{\mathrm{u}}^{\pm}$ are the elastic strains corresponding to the undamaged and completely damaged material, respectively. The superscript $\pm$ is $+$ in traction and $-$ in compression. The governing evolution parameter ε_{d} is set in a different way in traction and in compression. In fact, it is assumed that the damage in traction depends on the elastic stress, i.e. $\varepsilon_{\mathrm{d}} = \varepsilon_{\mathrm{e}}$, while in compression it depends on the total strain, i.e. $\varepsilon_{\mathrm{d}} = \varepsilon$. For a monotonic strain history, the evolutive equation (2) can be integrated, thus it takes the form:

$$D = \begin{cases} 0 & \text{for } \varepsilon_{\mathrm{d}} < \varepsilon_{\mathrm{c}}^{\pm}, \\ \dfrac{(\varepsilon_{\mathrm{c}}^{\pm} - \varepsilon_{\mathrm{d}})\varepsilon_{\mathrm{u}}^{\pm}}{\left(\varepsilon_{\mathrm{u}}^{\pm} - \varepsilon_{\mathrm{c}}^{\pm}\right)\varepsilon_{\mathrm{d}}} & \text{for } \varepsilon_{\mathrm{c}}^{\pm} < \varepsilon_{\mathrm{d}} < \varepsilon_{\mathrm{u}}^{\pm}, \\ 1 & \text{for } \varepsilon_{\mathrm{u}}^{\pm} < \varepsilon_{\mathrm{d}}. \end{cases} \tag{3}$$

The choice of assuming the damage in traction depending on the elastic strain allows one to limit the tensile stress within a prescribed value, for any plastic history, as schematically represented in Fig. 3. In fact, in Fig. 3, the stress–strain laws corresponding to three different strain paths are reported: path 1

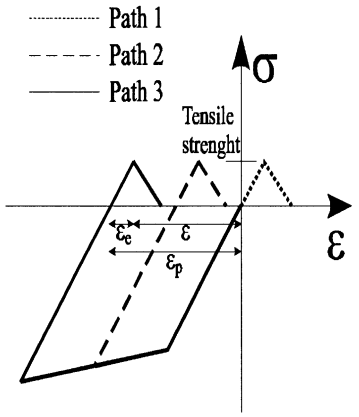

Fig. 3. Stress–strain for three possible strain paths.

considers a monotonic positive strain history, while paths 2 and 3 are referred to non monotonic negative strain histories.

2.1.2. Plasticity

Traction:

The mortar and block response in traction, i.e. for $\sigma \geqslant 0$, can be considered as purely cohesive, without any plastic effect. Thus, the plastic strain rate is set to be zero:

$$\dot{\varepsilon}_{\mathrm{p}} = 0 \quad \text{for } \sigma \geqslant 0 \tag{4}$$

Compression:

The mortar and block response in compression, i.e. for $\sigma < 0$, presents a damage-plastic behavior. Introducing the effective stress $\tilde{\sigma}$ as

$$\tilde{\sigma} = \frac{\sigma}{1-D}, \tag{5}$$

the following yield function with hardening is considered

$$f(\tilde{\sigma}, \alpha) = -\tilde{\sigma} - \left(\sigma_{\mathrm{y}} + K\alpha\right), \tag{6}$$

where α is the internal hardening variable, and K is the plastic hardening parameter. The evolutive equations are

$$\dot{\varepsilon}_{\mathrm{p}} = \dot{\lambda}\frac{\partial f}{\partial \tilde{\sigma}} = -\dot{\lambda}, \tag{7}$$

$$\dot{\alpha} = |\dot{\varepsilon}_{\mathrm{p}}| = -\dot{\varepsilon}_{\mathrm{p}}, \tag{8}$$

and the Kuhn–Tucker conditions result in

$$\dot{\varepsilon}_{\mathrm{p}} \leqslant 0 \quad f \leqslant 0 \quad \dot{\varepsilon}_{\mathrm{p}} f = 0. \tag{9}$$

The consistence law $\dot{\varepsilon}_{\mathrm{p}}\dot{f} = 0$ allows one to determine

$$\dot{\varepsilon}_{\mathrm{p}} = \frac{E}{E+K}\dot{\varepsilon} \quad \text{for } f = 0 \quad \text{with } \dot{\varepsilon}_{\mathrm{p}} \leqslant 0. \tag{10}$$

2.2. Composite

The composite material behavior is characterized by a linear elastic response with quite brittle failure. Several different strength criteria have been proposed in the literature, as reported for instance by Barbero (1999).

In the present work, the composite is considered as a linear elastic material with Young's modulus E_c until a brittle failure, i.e., the composite is assumed to collapse suddenly when the tensile or the compressive stress reaches a threshold stress f_R^+ in tension or f_R^+ in compression.

Moreover, the degradation is allowed also at the masonry–composite interface. The delamination of the composite sheet from the masonry element can be considered as brittle and mainly due to the shear fracture (i.e. mode II fracture) of the masonry, rather than to the damage of the glue.

It is assumed that at the virgin state, the adhesion between the laminate and the mortar is negligible, and thus, the FRP is perfectly glued only to the block. Hence, it is considered the presence of an initial defect of adhesion in correspondence of the mortar. The fracture propagation is ruled by the classical Griffith criterion, setting the critical release rate energy G_c as the one associate to the fracture mode II of the block material (Bazant and Planas, 1998).

Since the fracture evolution is coupled with the damage and plasticity, the energy release rate, for an infinitesimal delamination process inducing a variation dL_u of the unglued length, is given by

$$Gb\,\delta L_u = \delta W - \delta\mathscr{E} - \delta\Phi - \delta\Psi, \tag{11}$$

where δW is the external work performed during the process, $\delta\mathscr{E}$ is the elastic energy variation, $\delta\Phi$ and $\delta\Psi$ are energies dissipated for the plasticity and damage effects, respectively. Finally, delamination occurs when the energy release rate is equal to the critical energy G_c, i.e. when

$$G = G_c. \tag{12}$$

3. Reinforced masonry beam

The overall behavior of the reinforced masonry beam reported in Fig. 1 is derived developing a kinematical model which considers both elongation and bending deformations.

Let (x, y, ζ) be a Cartesian coordinate system such that ζ lies on the center-line axis of the undeformed beam, as reported in Fig. 2. The kinematics of the cross-section is defined by the elongation e and the curvature χ, such that the strain at a typical point of the beam is $\varepsilon = e + y\chi$.

In order to evaluate the overall behavior of the reinforced masonry beam, the unit cell is considered subjected to an axial force N_{tot} and to a bending moment M_{tot}. Simple kinematic observations allow us to deduce that the elongation and the curvature solution of the equilibrium problem both for the masonry and the reinforcement beams are piecewise constant. In fact, the block elongation and curvature are denoted by e_g and χ_g in the glued zone and by e_b and χ_b in the unglued zone, while the mortar elongation and curvature are set as e_m and χ_m. Analogously, the glued reinforcement elongation and curvature are e_g and χ_g while the unglued reinforcement elongation and curvature are e_u and χ_u. Summarizing, the elongations and curvatures are

	$0 < \zeta < L_g$	$L_g < \zeta < L_b$	$L_b < \zeta < L$
Masonry	$e_g\chi_g$	$e_b\chi_b$	$e_m\chi_m$
Reinforcement	$e_g\chi_g$	$e_u\chi_u$	$e_u\chi_u$

Note that the unglued reinforcement elongation and curvature e_u and χ_u can be evaluated as

$$\begin{aligned} e_{\mathrm{u}} &= \eta_{\mathrm{b}} e_{\mathrm{b}} + \eta_{\mathrm{m}} e_{\mathrm{m}}, \\ \chi_{\mathrm{u}} &= \eta_{\mathrm{b}} \chi_{\mathrm{b}} + \eta_{\mathrm{m}} \chi_{\mathrm{m}}, \end{aligned} \tag{13}$$

where $\eta_{\mathrm{b}} = \left(L_{\mathrm{b}} - L_{\mathrm{g}}\right)/L_{\mathrm{u}}$ and $\eta_{\mathrm{m}} = L_{\mathrm{m}}/L_{\mathrm{u}}$.

The reinforced masonry elongation e_{tot} and curvature χ_{tot} are determined as

$$\begin{aligned} e_{\mathrm{tot}} &= \frac{\left[e_{\mathrm{g}} L_{\mathrm{g}} + e_{\mathrm{b}}\ \left(L_{\mathrm{b}} - L_{\mathrm{g}}\right)\right] + e_{\mathrm{m}} L_{\mathrm{m}}}{L} = \frac{e_{\mathrm{g}} L_{\mathrm{g}} + e_{\mathrm{u}} L_{\mathrm{u}}}{L}, \\ \chi_{\mathrm{tot}} &= \frac{\left[\chi_{\mathrm{g}} L_{\mathrm{g}} + \chi_{\mathrm{b}}\ \left(L_{\mathrm{b}} - L_{\mathrm{g}}\right)\right] + \chi_{\mathrm{m}} L_{\mathrm{m}}}{L} = \frac{\chi_{\mathrm{g}} L_{\mathrm{g}} + \chi_{\mathrm{u}} L_{\mathrm{u}}}{L}. \end{aligned} \tag{14}$$

The resultants in the masonry beam, i.e. in the glued and unglued block and in the mortar, are

$$\begin{aligned} N_{\mathrm{g}}^{\mathrm{M}}\left(e_{\mathrm{g}}, \chi_{\mathrm{g}}\right) &= \int_{A_{\mathrm{M}}} \sigma_{\mathrm{g}}\left(e_{\mathrm{g}}, \chi_{\mathrm{g}}\right) \mathrm{d}A, \qquad M_{\mathrm{g}}^{\mathrm{M}}\left(e_{\mathrm{g}}, \chi_{\mathrm{g}}\right) = \int_{A_{\mathrm{M}}} y \sigma_{\mathrm{g}}\left(e_{\mathrm{g}}, \chi_{\mathrm{g}}\right) \mathrm{d}A, \\ N_{\mathrm{b}}(e_{\mathrm{b}}, \chi_{\mathrm{b}}) &= \int_{A_{\mathrm{M}}} \sigma_{\mathrm{b}}(e_{\mathrm{b}}, \chi_{\mathrm{b}}) \mathrm{d}A, \qquad M_{\mathrm{b}}(e_{\mathrm{b}}, \chi_{\mathrm{b}}) = \int_{A_{\mathrm{M}}} y \sigma_{\mathrm{b}}(e_{\mathrm{b}}, \chi_{\mathrm{b}}) \mathrm{d}A, \\ N_{\mathrm{m}}(e_{\mathrm{m}}, \chi_{\mathrm{m}}) &= \int_{A_{\mathrm{M}}} \sigma_{\mathrm{m}}(e_{\mathrm{m}}, \chi_{\mathrm{m}}) \mathrm{d}A, \qquad M_{\mathrm{m}}(e_{\mathrm{m}}, \chi_{\mathrm{m}}) = \int_{A_{\mathrm{M}}} y \sigma_{\mathrm{m}}(e_{\mathrm{m}}, \chi_{\mathrm{m}}) \mathrm{d}A. \end{aligned} \tag{15}$$

while the resultants in the glued and unglued parts of the composite reinforcement are

$$\begin{aligned} N_{\mathrm{g}}^{\mathrm{R}} &= A e_{\mathrm{g}} + B \chi_{\mathrm{g}}, \qquad M_{\mathrm{g}}^{\mathrm{R}} = B e_{\mathrm{g}} + D \chi_{\mathrm{g}}, \\ N_{\mathrm{u}} &= A e_{\mathrm{u}} + B \chi_{\mathrm{u}}, \qquad M_{\mathrm{u}} = B e_{\mathrm{u}} + D \chi_{\mathrm{u}}, \end{aligned} \tag{16}$$

where

$$A = A_{\mathrm{R}}^{+} + A_{\mathrm{R}}^{-}, \quad B = \frac{h}{2}\left(A_{\mathrm{R}}^{+} - A_{\mathrm{R}}^{-}\right), \quad D = \frac{h^2}{4}\left(A_{\mathrm{R}}^{+} + A_{\mathrm{R}}^{-}\right). \tag{17}$$

Taking into account relations (13), the second expression in Eq. (16) can be rewritten as

$$\begin{aligned} N_{\mathrm{u}} &= A\ \left(\eta_{\mathrm{b}} e_{\mathrm{b}} + \eta_{\mathrm{m}} e_{\mathrm{m}}\right) + B\ \left(\eta_{\mathrm{b}} \chi_{\mathrm{b}} + \eta_{\mathrm{m}} \chi_{\mathrm{m}}\right), \\ M_{\mathrm{u}} &= B\ \left(\eta_{\mathrm{b}} e_{\mathrm{b}} + \eta_{\mathrm{m}} e_{\mathrm{m}}\right) + D\ \left(\eta_{\mathrm{b}} \chi_{\mathrm{b}} + \eta_{\mathrm{m}} \chi_{\mathrm{m}}\right). \end{aligned} \tag{18}$$

The total resultant axial forces and the bending moments in the three parts of the reinforced masonry, represented in Fig. 2, are obtained as

$$\begin{aligned} N_1 &= N_{\mathrm{g}}^{\mathrm{M}} + N_{\mathrm{g}}^{\mathrm{R}}, \qquad M_1 = M_{\mathrm{g}}^{\mathrm{M}} + M_{\mathrm{g}}^{\mathrm{R}}, \\ N_2 &= N_{\mathrm{b}} + N_{\mathrm{u}}, \qquad M_2 = M_{\mathrm{b}} + M_{\mathrm{u}}, \\ N_3 &= N_{\mathrm{m}} + N_{\mathrm{u}}, \qquad M_3 = M_{\mathrm{m}} + M_{\mathrm{u}}. \end{aligned} \tag{19}$$

Finally, as the axial force and the bending moment are constant along the whole beam, the six equilibrium equations are

$$\begin{aligned} N_1 &= N_{\mathrm{tot}}, \quad M_1 = M_{\mathrm{tot}}, \\ N_2 &= N_{\mathrm{tot}}, \quad M_2 = M_{\mathrm{tot}}, \\ N_3 &= N_{\mathrm{tot}}, \quad M_3 = M_{\mathrm{tot}}. \end{aligned} \tag{20}$$

Regarding the delamination problem, the energy release rate G is evaluated from formula (11). The external work δW is determined as

$$\delta W = (N_{\mathrm{tot}}\delta\varepsilon_{\mathrm{tot}} + M_{\mathrm{tot}}\delta\chi_{\mathrm{tot}})L = \left(\delta W_{\mathrm{g}}^{\mathrm{M}} + \delta W_{\mathrm{b}} + \delta W_{\mathrm{m}} + \delta W_{\mathrm{g}}^{\mathrm{R}} + \delta W_{\mathrm{u}}\right), \tag{21}$$

where because of the virtual displacement theorem, it is

$$\begin{aligned}
\delta W_{\mathrm{g}}^{\mathrm{M}} &= \left[\int_{A_{\mathrm{M}}} \sigma_{\mathrm{g}}\delta\varepsilon_{\mathrm{g}}\,\mathrm{d}A\right]L_{\mathrm{g}},\\
\delta W_{\mathrm{b}} &= \left[\int_{A_{\mathrm{M}}} \sigma_{\mathrm{b}}\delta\varepsilon_{\mathrm{b}}\,\mathrm{d}A\right](L_{\mathrm{b}} - L_{\mathrm{g}}),\\
\delta W_{\mathrm{m}} &= \left[\int_{A_{\mathrm{M}}} \sigma_{\mathrm{m}}\delta\varepsilon_{\mathrm{m}}\,\mathrm{d}A\right]L_{\mathrm{m}},\\
\delta W_{\mathrm{g}}^{\mathrm{R}} &= \left(N_{\mathrm{g}}^{\mathrm{R}}\delta e_{\mathrm{g}} + M_{\mathrm{g}}^{\mathrm{R}}\delta\chi_{\mathrm{g}}\right)L_{\mathrm{g}},\\
\delta W_{\mathrm{u}} &= (N_{\mathrm{u}}\delta e_{\mathrm{u}} + M_{\mathrm{u}}\delta\chi_{\mathrm{u}})L_{\mathrm{u}}.
\end{aligned} \tag{22}$$

The elastic energy variation $\delta\mathscr{E}$ is computed as the sum of the energies stored in the block, in the mortar and in the reinforcement as follows:

$$\delta\mathscr{E} = \delta\left(\mathscr{E}_{\mathrm{g}}^{\mathrm{M}} + \mathscr{E}_{\mathrm{b}} + \mathscr{E}_{\mathrm{m}} + \mathscr{E}_{\mathrm{g}}^{\mathrm{R}} + \mathscr{E}_{\mathrm{u}}\right), \tag{23}$$

where

$$\begin{aligned}
\mathscr{E}_{\mathrm{g}}^{\mathrm{M}} &= \left[\tfrac{1}{2}\int_{A_{\mathrm{M}}} \sigma_{\mathrm{g}}(\varepsilon_{\mathrm{g}} - \varepsilon_{\mathrm{pg}})\,\mathrm{d}A\right]L_{\mathrm{g}},\\
\mathscr{E}_{\mathrm{b}} &= \left[\tfrac{1}{2}\int_{A_{\mathrm{M}}} \sigma_{\mathrm{b}}(\varepsilon_{\mathrm{b}} - \varepsilon_{\mathrm{pb}})\,\mathrm{d}A\right](L_{\mathrm{b}} - L_{\mathrm{g}}),\\
\mathscr{E}_{\mathrm{m}} &= \left[\tfrac{1}{2}\int_{A_{\mathrm{M}}} \sigma_{\mathrm{m}}(\varepsilon_{\mathrm{m}} - \varepsilon_{\mathrm{pm}})\,\mathrm{d}A\right]L_{\mathrm{m}},\\
\mathscr{E}_{\mathrm{g}}^{\mathrm{R}} &= \tfrac{1}{2}\left(N_{\mathrm{g}}^{\mathrm{R}}e_{\mathrm{g}} + M_{\mathrm{g}}^{\mathrm{R}}\chi_{\mathrm{g}}\right)L_{\mathrm{g}},\\
\mathscr{E}_{\mathrm{u}} &= \tfrac{1}{2}(N_{\mathrm{u}}e_{\mathrm{u}} + M_{\mathrm{u}}\chi_{\mathrm{u}})L_{\mathrm{u}}.
\end{aligned} \tag{24}$$

The dissipation due to plasticity and damage is given by

$$\delta\Phi + \delta\Psi = \left(\delta\Phi_{\mathrm{g}}^{\mathrm{M}} + \delta\Phi_{\mathrm{b}} + \delta\Phi_{\mathrm{m}}\right) + \left(\delta\Psi_{\mathrm{g}}^{\mathrm{M}} + \delta\Psi_{\mathrm{b}} + \delta\Psi_{\mathrm{m}}\right), \tag{25}$$

where

$$\begin{aligned}
&\delta\Phi_{\mathrm{g}}^{\mathrm{M}} = \left[\int_{A_{\mathrm{M}}} \sigma_{\mathrm{g}}\delta\varepsilon_{\mathrm{pg}}\,\mathrm{d}A\right]L_{\mathrm{g}}, \quad \delta\Psi_{\mathrm{g}}^{\mathrm{M}} = \left[\frac{1}{2}\int_{A_{\mathrm{M}}} \sigma_{\mathrm{g}}(\varepsilon_{\mathrm{g}} - \varepsilon_{\mathrm{pg}})\delta D_{\mathrm{g}}\,\mathrm{d}A\right]L_{\mathrm{g}},\\
&\delta\Phi_{\mathrm{b}} = \left[\int_{A_{\mathrm{M}}} \sigma_{\mathrm{b}}\delta\varepsilon_{\mathrm{pb}}\,\mathrm{d}A\right](L_{\mathrm{b}} - L_{\mathrm{g}}), \quad \delta\Psi_{\mathrm{b}} = \left[\frac{1}{2}\int_{A_{\mathrm{M}}} \sigma_{\mathrm{b}}(\varepsilon_{\mathrm{b}} - \varepsilon_{\mathrm{pb}})\delta D_{\mathrm{b}}\,\mathrm{d}A\right](L_{\mathrm{b}} - L_{\mathrm{g}}),\\
&\delta\Phi_{\mathrm{m}} = \left[\int_{A_{\mathrm{M}}} \sigma_{\mathrm{m}}\delta\varepsilon_{\mathrm{pm}}\,\mathrm{d}A\right]L_{\mathrm{m}}, \quad \delta\Psi_{\mathrm{m}} = \left[\frac{1}{2}\int_{A_{\mathrm{M}}} \sigma_{\mathrm{m}}(\varepsilon_{\mathrm{m}} - \varepsilon_{\mathrm{pm}})\delta D_{\mathrm{m}}\,\mathrm{d}A\right]L_{\mathrm{m}}.
\end{aligned}$$

Finally, the delamination is governed by Eq. (12).

Because of the damage, the plasticity, the brittle failure of the reinforcement and the possible delamination of the composite from the masonry, the solution of Eq. (20) is not straightforward. Thus, analytical solutions are possible only in few very special and simple cases. In general, the overall stress–strain

$(N_{\mathrm{tot}}, M_{\mathrm{tot}}) - (e_{\mathrm{tot}}, \chi_{\mathrm{tot}})$ relationships can be computed numerically, and thus a computational procedure is proposed in the following.

4. Computational procedure

4.1. Damage and plasticity

The nonlinear relations between the kinematic parameters and the stress resultants are solved developing a numerical procedure. To this end, initially the expressions in Eq. (20) are written in the equivalent residual form:

$$\begin{aligned}
R_1 &= N_1 - N_{\mathrm{tot}} = N_{\mathrm{g}}^{\mathrm{M}} + N_{\mathrm{g}}^{\mathrm{R}} - N_{\mathrm{tot}} = 0,\\
R_2 &= M_1 - M_{\mathrm{tot}} = M_{\mathrm{g}}^{\mathrm{M}} + M_{\mathrm{g}}^{\mathrm{R}} - M_{\mathrm{tot}} = 0,\\
R_3 &= N_2 - N_{\mathrm{tot}} = N_{\mathrm{b}} + N_{\mathrm{u}} - N_{\mathrm{tot}} = 0,\\
R_4 &= M_2 - M_{\mathrm{tot}} = M_{\mathrm{b}} + M_{\mathrm{u}} - M_{\mathrm{tot}} = 0,\\
R_5 &= N_3 - N_{\mathrm{tot}} = N_{\mathrm{m}} + N_{\mathrm{u}} - N_{\mathrm{tot}} = 0,\\
R_6 &= M_3 - M_{\mathrm{tot}} = M_{\mathrm{m}} + M_{\mathrm{u}} - M_{\mathrm{tot}} = 0.
\end{aligned} \tag{26}$$

Introducing the residual vector $\mathbf{R}$ and the deformation vector $\mathbf{e}$ as

$$\mathbf{R} = \begin{Bmatrix} R_1\\ R_2\\ R_3\\ R_4\\ R_5\\ R_6 \end{Bmatrix}, \qquad \mathbf{e} = \begin{Bmatrix} e_{\mathrm{g}}\\ \chi_{\mathrm{g}}\\ e_{\mathrm{b}}\\ \chi_{\mathrm{b}}\\ e_{\mathrm{m}}\\ \chi_{\mathrm{m}} \end{Bmatrix},$$

the expressions in Eq. (26) can be rewritten in compact form as

$$\mathbf{R}(\mathbf{e}) = \mathbf{0}. \tag{27}$$

In the following, Eq. (27) is solved using a Newton algorithm (Luenberger, 1973):

$$\mathbf{R}\left(\mathbf{e}^{k+1}\right) = \mathbf{R}\left(\mathbf{e}^{k}\right) + \mathbf{K}_{\mathrm{t}}\ \left(\mathbf{e}^{k+1} - \mathbf{e}^{k}\right), \tag{28}$$

where the superscripts k and $k+1$ indicate the iteration indices and the tangent matrix is

$$\mathbf{K}_{\mathrm{t}} = \left.\frac{\partial \mathbf{R}}{\partial \mathbf{e}}\right|_{\mathbf{e}=\mathbf{e}^{k}}. \tag{29}$$

Given the kth solution, i.e. $\mathbf{e}^{k}$, Eq. (28) can be solved in terms of $\mathbf{e}^{k+1}$. The derivative of the residuals is the tangent operator of the equilibrium problem (27), and it is explicitly expressed as

$$\mathbf{K}_{\mathrm{t}} = \begin{bmatrix} A + A_{\mathrm{g}} & B + B_{\mathrm{g}} & 0 & 0 & 0 & 0\\ B + B_{\mathrm{g}} & D + D_{\mathrm{g}} & 0 & 0 & 0 & 0\\ 0 & 0 & A_{\mathrm{b}} + A\eta_{\mathrm{b}} & B_{\mathrm{b}} + B\eta_{\mathrm{b}} & A\eta_{\mathrm{m}} & B\eta_{\mathrm{m}}\\ 0 & 0 & B_{\mathrm{b}} + B\eta_{\mathrm{b}} & D_{\mathrm{b}} + D\eta_{\mathrm{b}} & B\eta_{\mathrm{m}} & D\eta_{\mathrm{m}}\\ 0 & 0 & A\eta_{\mathrm{b}} & B\eta_{\mathrm{b}} & A\eta_{\mathrm{m}} + A_{\mathrm{m}} & B\eta_{\mathrm{m}} + B_{\mathrm{m}}\\ 0 & 0 & B\eta_{\mathrm{b}} & D\eta_{\mathrm{b}} & B\eta_{\mathrm{m}} + B_{\mathrm{m}} & D\eta_{\mathrm{m}} + D_{\mathrm{m}} \end{bmatrix}, \tag{30}$$

where

$$
\begin{aligned}
A_{\mathrm{g}} &= \frac{\partial N_{\mathrm{g}}^{\mathrm{M}}}{\partial e_{\mathrm{g}}} = \int_{A_{\mathrm{M}}} \frac{\partial \sigma_{\mathrm{g}}}{\partial e_{\mathrm{g}}}\,\mathrm{d}A,\\
B_{\mathrm{g}} &= \frac{\partial N_{\mathrm{g}}^{\mathrm{M}}}{\partial \chi_{\mathrm{g}}} = \int_{A_{\mathrm{M}}} \frac{\partial \sigma_{\mathrm{g}}}{\partial \chi_{\mathrm{g}}}\,\mathrm{d}A = \frac{\partial M_{\mathrm{g}}^{\mathrm{M}}}{\partial e_{\mathrm{g}}} = \int_{A_{\mathrm{M}}} y\frac{\partial \sigma_{\mathrm{g}}}{\partial e_{\mathrm{g}}}\,\mathrm{d}A,\\
D_{\mathrm{g}} &= \frac{\partial M_{\mathrm{g}}^{\mathrm{M}}}{\partial \chi_{\mathrm{g}}} = \int_{A_{\mathrm{M}}} y\frac{\partial \sigma_{\mathrm{g}}}{\partial \chi_{\mathrm{g}}}\,\mathrm{d}A.
\end{aligned}
\tag{31}
$$

$$
\begin{aligned}
A_{\mathrm{b}} &= \frac{\partial N_{\mathrm{b}}}{\partial e_{\mathrm{b}}} = \int_{A_{\mathrm{M}}} \frac{\partial \sigma_{\mathrm{b}}}{\partial e_{\mathrm{b}}}\,\mathrm{d}A,\\
B_{\mathrm{b}} &= \frac{\partial N_{\mathrm{b}}}{\partial \chi_{\mathrm{b}}} = \int_{A_{\mathrm{M}}} \frac{\partial \sigma_{\mathrm{b}}}{\partial \chi_{\mathrm{b}}}\,\mathrm{d}A = \frac{\partial M_{\mathrm{b}}}{\partial e_{\mathrm{b}}} = \int_{A_{\mathrm{M}}} y\frac{\partial \sigma_{\mathrm{b}}}{\partial e_{\mathrm{b}}}\,\mathrm{d}A,\\
D_{\mathrm{b}} &= \frac{\partial M_{\mathrm{b}}}{\partial \chi_{\mathrm{b}}} = \int_{A_{\mathrm{M}}} y\frac{\partial \sigma_{\mathrm{b}}}{\partial \chi_{\mathrm{b}}}\,\mathrm{d}A.
\end{aligned}
\tag{32}
$$

$$
\begin{aligned}
A_{\mathrm{m}} &= \frac{\partial N_{\mathrm{m}}}{\partial e_{\mathrm{m}}} = \int_{A_{\mathrm{M}}} \frac{\partial \sigma_{\mathrm{m}}}{\partial e_{\mathrm{m}}}\,\mathrm{d}A,\\
B_{\mathrm{m}} &= \frac{\partial N_{\mathrm{m}}}{\partial \chi_{\mathrm{m}}} = \int_{A_{\mathrm{M}}} \frac{\partial \sigma_{\mathrm{m}}}{\partial \chi_{\mathrm{m}}}\,\mathrm{d}A = \frac{\partial M_{\mathrm{m}}}{\partial e_{\mathrm{m}}} = \int_{A_{\mathrm{M}}} y\frac{\partial \sigma_{\mathrm{m}}}{\partial e_{\mathrm{m}}}\,\mathrm{d}A,\\
D_{\mathrm{m}} &= \frac{\partial M_{\mathrm{m}}}{\partial \chi_{\mathrm{m}}} = \int_{A_{\mathrm{M}}} y\frac{\partial \sigma_{\mathrm{m}}}{\partial \chi_{\mathrm{m}}}\,\mathrm{d}A.
\end{aligned}
\tag{33}
$$

It can be noted that the tangent matrix is not symmetric. This fact is due to the particular choice of the equilibrium equations that are not conjugate to the kinematic parameters considered. As the number of degrees of freedom is very low (it is equal to six), the lack of symmetry of $\mathbf{K}_{\mathrm{t}}$ does not generate any numerical burden.

The computation of $\mathbf{R}$ and of its derivatives requires

- the time integration of the local constitutive equations,
- the determination of the algorithmically tangent moduli,
- the evaluation of the integrals over the cross-section A_{M}.

The time integration of Eqs. (2)–(10) in the interval $[t_n, t_{n+1}]$ is performed adopting a backward-Euler scheme (Simo and Hughes, 1998). To simplify the notation, the subscript "n" indicates a quantity evaluated at time t_n while no subscript indicates a quantity evaluated at time t_{n+1}.

4.1.1. Damage

Once the evolution parameter ε_{d} is given, the damage variable is computed, according to the formula

$$
D = \begin{cases} 0 & \text{for } \varepsilon_{\mathrm{d}} < \varepsilon_{\mathrm{c}}^{\pm},\\ \max\left(D_n, \frac{(\varepsilon_{\mathrm{c}}^{\pm}-\varepsilon_{\mathrm{d}})\varepsilon_{\mathrm{u}}^{\pm}}{(\varepsilon_{\mathrm{u}}^{\pm}-\varepsilon_{\mathrm{c}}^{\pm})\varepsilon_{\mathrm{d}}}\right) & \text{for } \varepsilon_{\mathrm{c}}^{\pm} < \varepsilon_{\mathrm{d}} < \varepsilon_{\mathrm{u}}^{\pm},\\ 1 & \text{for } \varepsilon_{\mathrm{u}}^{\pm} < \varepsilon_{\mathrm{d}}. \end{cases}
\tag{34}
$$

4.1.2. Plasticity

The time discrete model is solved using a return map algorithm, as described in Simo and Hughes (1998). It is set as

$$\lambda = \int_{t_n}^{t_{n+1}} \dot{\varepsilon}_{\mathrm{p}}\,\mathrm{d}t = \varepsilon_{\mathrm{p}} - \varepsilon_{\mathrm{p},n}. \tag{35}$$

Then, the algorithm consists of two steps, i.e. the predictor and corrector phases, which are schematically reported:

Predictor phase:

$\widetilde{\sigma}^t = E(\varepsilon - \varepsilon_{\mathrm{p},n})$
$\varepsilon_{\mathrm{p}}^t = \varepsilon_{\mathrm{p},n}$
$\alpha^t = \alpha_n$
$f^t = -\widetilde{\sigma}^t - (\sigma_{\mathrm{y}} + K\alpha^t)$

Corrector phase:

If $f^t < 0$ elastic step
$\varepsilon_{\mathrm{p}} = \varepsilon_{\mathrm{p}}^t$
$\alpha = \alpha^t$
$\widetilde{\sigma} = \widetilde{\sigma}^t$
Elseif $f^t \geqslant 0$ plastic step
$\lambda = -f^t/(E+K)\ (f=0)$
$\varepsilon_{\mathrm{p}} = \varepsilon_{\mathrm{p},n} + \lambda$
$\alpha = \alpha_n - \lambda$
$\widetilde{\sigma} = \widetilde{\sigma}^t - E\lambda$
Endif

4.1.3. Algorithmic tangent

Because of Eq. (5), it results that

$$\sigma = (1-D)\widetilde{\sigma}.$$

Thus, the algorithmically tangent moduli $\partial\sigma/\partial e$ and $\partial\sigma/\partial\chi$ are computed as

$$\begin{aligned}
\frac{\partial\sigma}{\partial e} &= \frac{\partial\sigma}{\partial\widetilde{\sigma}}\frac{\partial\widetilde{\sigma}}{\partial e} + \frac{\partial\sigma}{\partial D}\frac{\partial D}{\partial e} = (1-D)\frac{\partial\widetilde{\sigma}}{\partial e} - \widetilde{\sigma}\frac{\partial D}{\partial e} = E_{\mathrm{T}},\\
\frac{\partial\sigma}{\partial\chi} &= \frac{\partial\sigma}{\partial\widetilde{\sigma}}\frac{\partial\widetilde{\sigma}}{\partial\chi} + \frac{\partial\sigma}{\partial D}\frac{\partial D}{\partial\chi} = (1-D)\frac{\partial\widetilde{\sigma}}{\partial\chi} - \widetilde{\sigma}\frac{\partial D}{\partial\chi} = y\,E_{\mathrm{T}},
\end{aligned} \tag{36}$$

where

$$E_{\mathrm{T}} = (1-D)\frac{E\,K}{E+K} - \widetilde{\sigma}\frac{\varepsilon_{\mathrm{c}}^{\pm}\varepsilon_{\mathrm{u}}^{\pm}}{(\varepsilon_{\mathrm{u}}^{\pm} - \varepsilon_{\mathrm{c}}^{\pm})\varepsilon_{\mathrm{d}}^2}. \tag{37}$$

A tangent–secant modulus can be introduced by setting

$$E_{\mathrm{T}} = (1-D)\frac{E\,K}{E+K} \tag{38}$$

that can be regarded as tangent with respect to the plasticity equations and as secant with respect to the damage evolution.

The substitution of tangent modulus (37) or tangent–secant modulus (38) into Eqs. (31)–(33) returns the explicit form for the quantities A_*, B_* and D_*, where the subscript '$*$' stands for 'g', 'b' or 'm':

$$A_* = \int_{A_M} E_T \, dA \quad B_* = \int_{A_M} y E_T \, dA \quad D_* = \int_{A_M} y^2 E_T \, dA. \tag{39}$$

Finally, the integration over the cross-section to determine the residuals **R** and its derivatives is performed by discretizing the cross-section in stripes and applying the Gauss integration formula within each stripe.

4.2. Delamination

As described in the previous sections, it is assumed that adhesion between the masonry and the reinforcement is present only in the glued part of the reinforced masonry beam having length L_g, while the unglued part has length L_u. Delamination effect is accounted for considering the variation of the size L_u during the loading history.

The procedure proposed for evaluating the delamination effect is based on the Griffith criterion, through a discretization of the evolutive equation (12) according to a finite difference scheme, in the framework of the virtual crack method. Hence, at each time step the algorithm consists of the following scheme:

1. Let L_u be the actual delaminated size.
2. Set $L_{u1} = L_u$.
3. Compute the response of the reinforced masonry beam, for the assigned value of L_{u1}:
   Compute the $(N_{tot}, M_{tot})_1 - (e_{tot}, \chi_{tot})_1$ relationship.
   Compute the elastic energy $\mathscr{E}_1$.
4. If $L_{u1} < L$, set $L_{u2} = L_{u1} + \Delta L$.
5. Compute the response of the reinforced masonry beam, for the assigned value of L_{u2}:
   Compute the $(N_{tot}, M_{tot})_2 - (e_{tot}, \chi_{tot})_2$ relationship.
   Compute the elastic energy $\mathscr{E}_2$.
6. Compute the finite variation of the external work ΔW (Eq. (21)) and of the dissipation $\Delta \Phi + \Delta \Psi$ (Eq. (25)).
7. Evaluate the elastic energy rate as finite difference
$$\Delta \mathscr{E} = \mathscr{E}_2 - \mathscr{E}_1. \tag{40}$$
8. Determine the energy release rate G as
$$Gb\Delta L = \Delta W - \Delta \mathscr{E} - \Delta \Phi - \Delta \Psi. \tag{41}$$
9. If $G < G_c$, there is not delamination, thus the delaminated size is L_{u1} and the overall reinforced masonry response is given by the relationship $(N_{tot}, M_{tot})_1 - (e_{tot}, \chi_{tot})_1$. If $G \geqslant G_c$, delamination occurs, thus the delaminated size is L_{u2} and the overall reinforced masonry response is given by the relationship $(N_{tot}, M_{tot})_2 - (e_{tot}, \chi_{tot})_2$.

4.3. Control parameters

The softening behavior of the mortar and block can induce an overall response of the reinforced masonry characterized by steep softening branches and possibly also by snapbacks. In particular, strain and damage concentration occurs first in the mortar, since it is generally the weakest component of the masonry, than in the block. Hence, it appears convenient to adopt an arc-length method to catch the overall material response. Hence, the cylindrical as well as the linearized arc-length methods (Crisfield, 1991) with local control are developed for the particular problem under consideration. Some investigations have been

performed in order to individuate the most convenient strain parameters to control within the arc-length technique. Finally, the nine parameters chosen are the strain increments at the top, at the bottom and at the neutral axis, in the mortar and in the glued and the unglued parts of the block:

$$\begin{aligned}
&\text{top} && \Delta\varepsilon_*^{\text{top}} = \Delta e_* - \tfrac{h}{2}\,\Delta\chi_*,\\
&\text{bottom} && \Delta\varepsilon_*^{\text{bot}} = \Delta e_* + \tfrac{h}{2}\,\Delta\chi_*,\\
&\text{neutral axis} && \Delta\varepsilon_*^{n\text{-}ax} = \Delta e_* + Yn_*\,\Delta\chi_*,
\end{aligned}$$

where $Yn_* = -e_*/\chi_*$ and the subscript '$*$' stands for 'g', 'b' or 'm'.

4.4. Algorithm summary

The algorithmic implementation of the iterative procedure relative to the scheme above presented is briefly reported:

```
do loop on time history
  do while (residuals ⩽ tolerance)
    initialize quantities
    do loop on delamination
      masonry beam
      loop on the elements in the cross section
        loop on the Gauss points
      compute total strain ε
      compute plastic strain ε_p
      compute damage D
      compute stress σ
      compute N_g^M, N_b, N_m and M_g^M, M_b, M_m
      add contribution to N_tot and M_tot
      compute algorithmic tangent moduli
      add contribution to global tangent
        end loop
      end loop
      reinforcement beam
      compute N_g^R, N_u and M_g^R, M_u
      add contribution to N_tot and M_tot
      compute reinforcement elastic energy
      compute stiffness matrix
      add contribution to global tangent
      compute residuals
      solve system
      compute the load increment (arc-length method)
      compute new solution e, χ
    end loop for nonlinear problem
    compute release energy rate as finite difference
    check delamination
  end loop on delamination
  check reinforcement failure
  increase the time
end loop on time
```

5. Numerical applications

Applications are developed for a reinforced masonry element characterized by mortar and block with the following material properties:

Mortar:

$$E_{\mathrm{m}} = 5000 \text{ MPa} \quad \sigma_{\mathrm{y,m}} = 3 \text{ MPa} \quad K_{\mathrm{m}} = 500 \text{ MPa}$$
$$\varepsilon^{+}_{\mathrm{c,m}} = 1E-4 \quad \varepsilon^{+}_{\mathrm{u,m}} = 4E-4 \quad \varepsilon^{-}_{\mathrm{c,m}} = 10E-4 \quad \varepsilon^{-}_{\mathrm{u,m}} = 40E-4.$$

Block:

$$E_{\mathrm{b}} = 15{,}000 \text{ MPa} \quad \sigma_{\mathrm{y,b}} = 10 \text{ MPa} \quad K_{\mathrm{b}} = 1500 \text{ MPa}$$
$$\varepsilon^{+}_{\mathrm{c,b}} = 1E-4 \quad \varepsilon^{+}_{\mathrm{u,b}} = 6E-4 \quad \varepsilon^{-}_{\mathrm{c,b}} = 15E-4 \quad \varepsilon^{-}_{\mathrm{u,b}} = 60E-4.$$

The masonry geometrical parameters are

$$L_{\mathrm{b}} = 25 \text{ mm}, \; L_{\mathrm{m}} = 5 \text{ mm}, \; b = 130 \text{ mm}, \; h = 250 \text{ mm}$$

which correspond to a typical masonry with blocks $50 \times 130 \times 250$ mm^3 and mortar layers of 10 mm width.

In Fig. 4 the stress–strain response for the block, the mortar and the homogenized masonry is plotted.

It can be noted that the response of the masonry is significantly worse than the response of the two components. In fact, it presents the same tensile and compressive strength of the mortar, which is generally lower than the strength of the block. Moreover, the masonry behavior is characterized by a steeper softening branch than the two components. This is due to the fact that when the masonry is subjected to a load history the deformation localizes in the mortar as it is the weakest component.

A carbon fiber-reinforced plastic composite material with Young's modulus $E_{\mathrm{c}} = 200{,}000$ MPa is considered. Note that, although the strength of the FRP sheets is generally different in traction and in compression, in the application developed in the following, it is set $f^{+}_{\mathrm{R}} = f^{-}_{\mathrm{R}} = 2500$ MPa. It is assumed partially glued to the masonry so that $L_{\mathrm{g}} = 22$ mm.

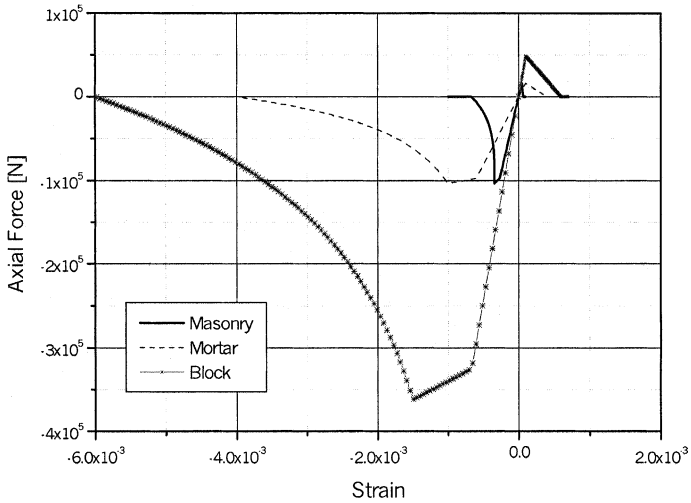

Fig. 4. Stress–strain relation for the mortar, the block and the masonry materials.

5.1. Axial behavior

Initially, the axial response of the reinforced masonry is investigated, neglecting the possible delamination. In Figs. 5 and 6 the axial force N_{tot} versus the strain e_{tot} is plotted in tension and in compression, respectively, for different values of the reinforcement area, with $A_R = A_R^+ = A_R^-$.

It can be noted that the presence of the reinforcement improves the mechanical response of the masonry. In fact, the plain masonry is not able to carry any load when the mortar is completely damaged, as represented in Figs. 5 and 6 for $A_R = 0$ mm^2. On the contrary, the reinforcement allows to transfer the external axial force to the block, also when the mortar is completely damaged. Moreover, the strain localization in the mortar is reduced by increasing the FRP area, thus the material becomes more ductile, and the softening branch results less steep.

In Figs. 5 and 6 the analysis is performed until the complete damage of the mortar is reached, thus it does not describe the whole strength capability of the reinforced masonry. In fact, the analysis can be carried on until the collapse of the block and of the reinforcement occurs, as shown in Figs. 7 and 8, where the total axial force N_{tot} is plotted versus the strain e_{tot} in tension and in compression, respectively, for $A_R = A_R^+ = A_R^- = 20$ mm^2.

Note that in the curve represented in Fig. 7, the collapse in tension of the reinforcement, reached for $N_{tot} = f_R^+ \, 2A_R = 100,000$ N occurs when the glued block and the mortar are both completely damaged, and it corresponds to a value out of the represented scale. On the other hand, the reinforcement failure in compression occurs for $N_{tot} = -f_R^- \, 2A_R = -100,000$ N when only the mortar is completely damaged, as shown in Fig. 8. Thus, it can be pointed out that the reinforced masonry tensile response is characterized by a softening branch and a severe snapback, which occur during the damage and failure of the mortar and of the glued block, respectively. The compressive response is characterized by a softening branch, representing the mortar degradation. In Fig. 8, the axial force–strain relation, obtained neglecting the reinforcement failure, is plotted with a dashed line. Even in this case the snapback occurs during the damage of the glued block. The unglued part of the block does not undergo any damage during the loading history, as it remains unloaded, when the mortar is completely damaged.

The collapse load in tension for a reinforced masonry with $A_R = 20$ mm^2 is almost ten times higher than the collapse load for the plain masonry, represented in Fig. 5 (see case $A_R = 0$ mm^2). On the contrary, the

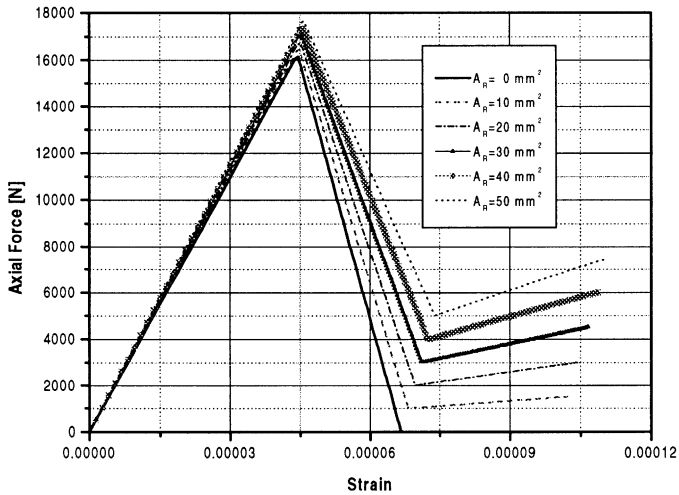

Fig. 5. Axial force–strain in tension for different amounts of FRP reinforcement.

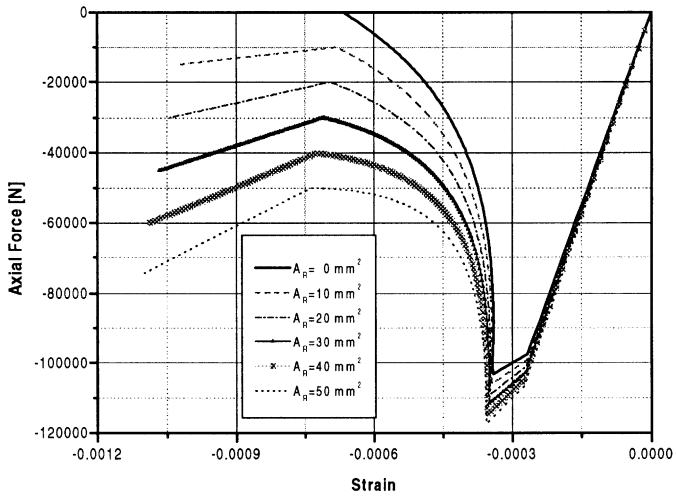

Fig. 6. Axial force–strain relation in compression for different amounts of FRP reinforcement.

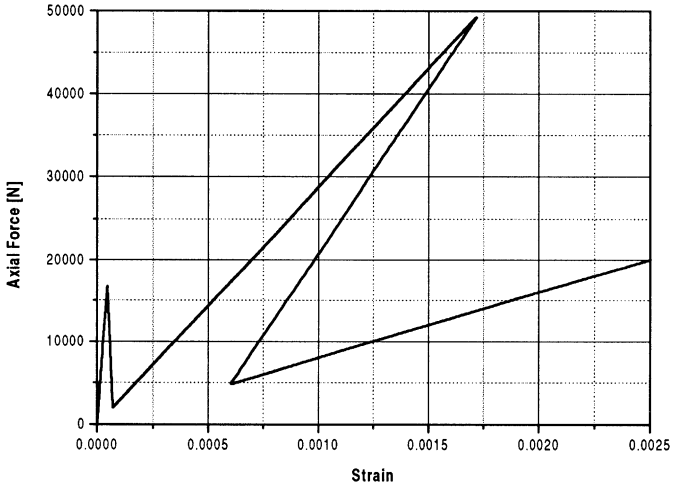

Fig. 7. Axial force–strain in tension for $A_R = 20$ mm^2.

collapse load in compression is almost the same for the reinforced and unreinforced masonry (see Fig. 6 for $A_R = 0$ mm^2), because of the satisfactory mechanical properties of the mortar and block in compression.

From a computational point of view, it can be emphasized that the procedure developed is able to describe the complex response of the reinforced masonry characterized by softening and snapbacks. In fact, the developed arc-length technique demonstrates satisfactory convergence properties.

5.2. Bending behavior

Then, the bending behavior is studied. Initially, the delamination effects are disregarded. In Fig. 9, the total bending moment M_{tot} is plotted versus the curvature χ_{tot} for different amounts of FRP reinforcement,

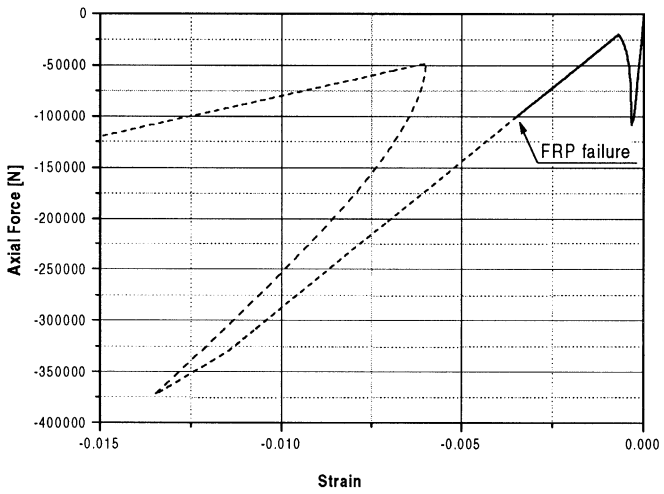

Fig. 8. Axial force–strain in compression for $A_R = 20$ mm^2.

during the initial damage of the mortar. As for the axial problem, also for the bending case it is apparent the beneficial effects of the reinforcement in improving the mechanical response, and in particular the ductility, of the masonry.

The results of a complete bending analysis, performed taking into account the whole nonlinear behavior of the mortar and block, are reported in Figs. 9–11.

In particular, in Fig. 10 the bending moment M_{tot} is plotted versus the curvature χ_{tot} for $A_R = A_R^+ = A_R^- = 20$ mm^2. The mechanical response of the material is characterized by different severe snapbacks due to the damage and failure of the mortar and of the block. The curve reported does not show the reinforcement failure that occurs when $M_{tot} = f_R A_R h = 12,500,000$ N mm. The collapse bending moment for a reinforced masonry with $A_R = 20$ mm^2 is more than ten times higher than the collapse load for the plain masonry, represented in Fig. 9 (see case $A_R = 0$ mm^2).

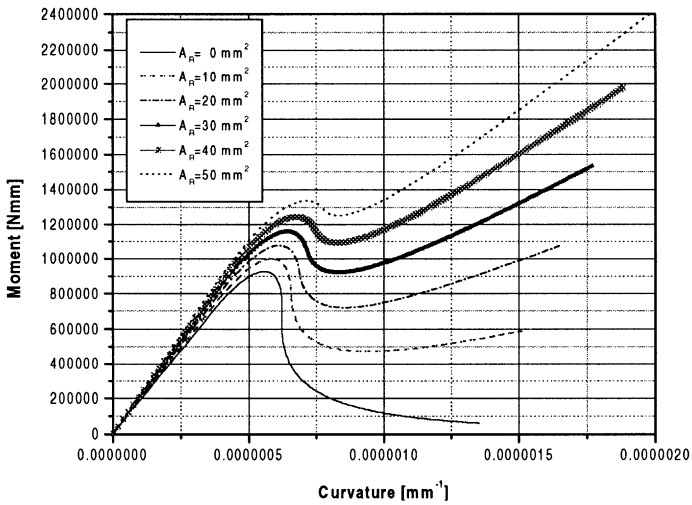

Fig. 9. Bending moment–curvature relation for different amounts of FRP reinforcement.

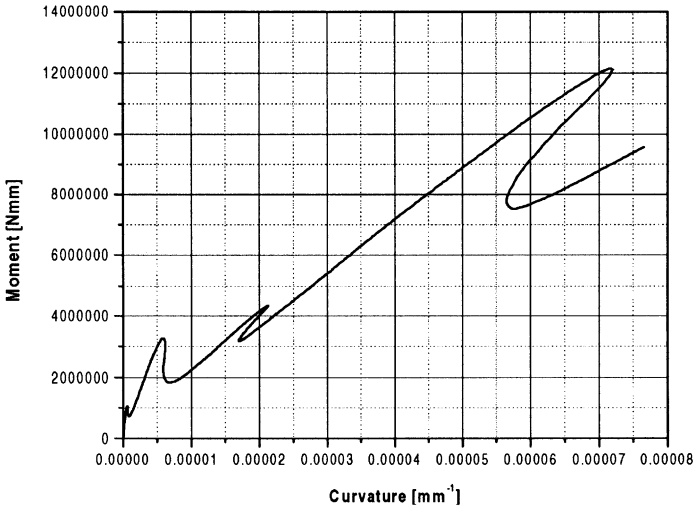

Fig. 10. Bending moment–curvature relation for $A_R = 20$ mm^2.

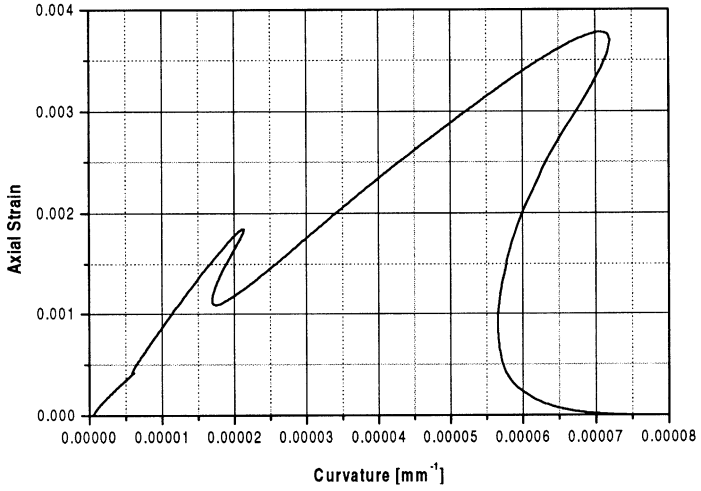

Fig. 11. Axial strain–curvature relation for the bending load history with $A_R = 20$ mm^2.

In Fig. 11, the axial strain is plotted versus the curvature for the bending load history. It can be pointed out that even for a monotonic bending load the axial strain is different from zero because of the damage and the plastic processes that occur in the masonry. In Fig. 12, the neutral axes in the glued block $Yn_g = -e_g/\chi_g$, in the unglued block $Yn_b = -e_b/\chi_b$, in the mortar $Yn_m = -e_m/\chi_m$ and the overall neutral axis $Yn_{tot} = -e_{tot}/\chi_{tot}$ are plotted versus time. Some considerations can be made. At the beginning of the analysis, the mortar starts to damage in tension, so the neutral axis Yn_m tends to move towards the top of the section, reducing the are in compression. This effect produces an extension of the mortar which is constrained by the presence of the reinforcement; thus a compression state in the close unglued block is induced. As a consequence, the axis Yn_b tends towards the bottom of the section as the unglued block still behaves elastically. When the mortar reaches the complete damage, Yn_m goes back to zero and Yn_b suddenly drops to zero, too.

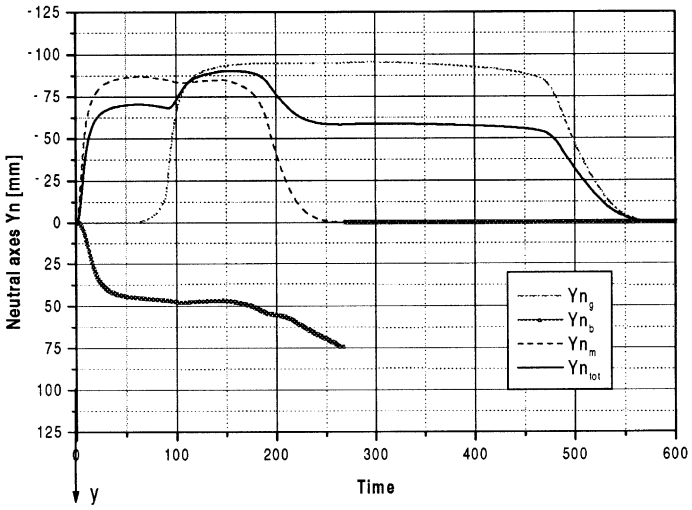

Fig. 12. Position of the neutral axes versus time for the bending load history with $A_R = 20$ mm^2.

The neutral axis Yn_g starts to move from the section center later than Yn_m and Yn_b when the glued block begins to damage. The position Yn_{tot} of the overall axis is influenced by the movements of Yn_m, Yn_b and Yn_g and, at the end of the analysis, it tends to zero since only the reinforcement remains undamaged.

5.3. Delamination

Two different values of the critical energy release rate governing the delamination phenomenon are assumed $G_c = 0.002$–0.04 N/mm; these values correspond to possible critical energies for the block in mode II. In Fig. 13, the axial force N_{tot} is plotted versus the strain e_{tot} in compression using lines for different fixed values of the glued length L_g of the reinforcement. In the same figure, the axial force–strain relation, which

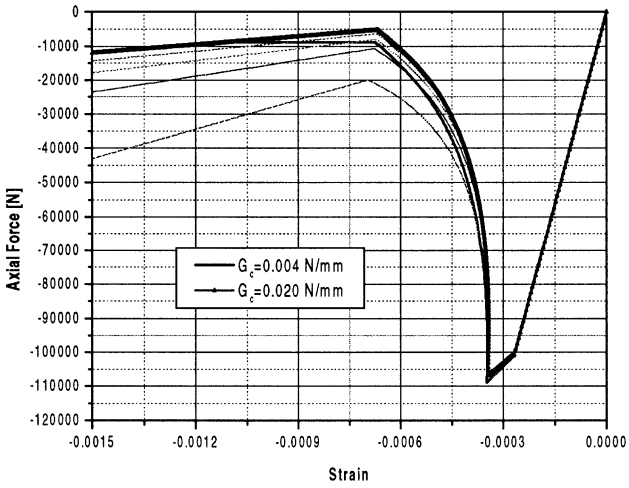

Fig. 13. Delamination process in compression.

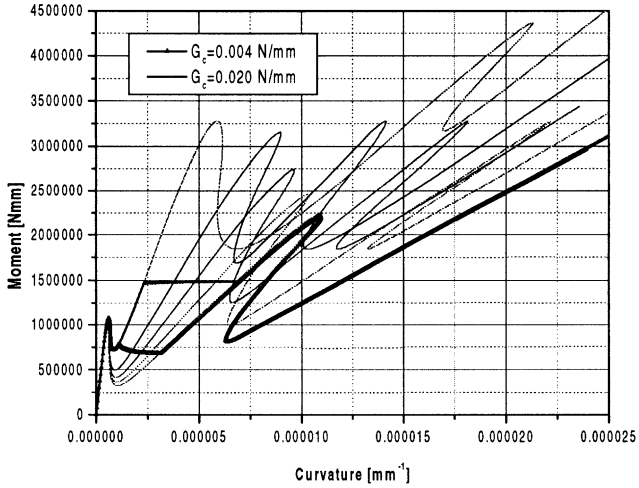

Fig. 14. Delamination process in bending.

takes into account the delamination process, is represented with a thick line. The delamination occurs during the mortar damage, when the block still behaves elastically.

In Fig. 14, the bending moment M_{tot} is plotted versus the curvature χ_{tot} for different fixed values of L_{g} with thin lines, while the two curves with thick lines represent the material response taking into account the delamination process for two different values of the fracture energy G_{c}. It can be pointed out the significative influence of the delamination effects on the mechanical response of the reinforced masonry. Of course, it results that for higher values of the fracture energy the delamination occurs later.

6. Conclusion

A one-dimensional elasto-plastic damage model for the reinforced masonry is proposed. In particular, a homogenization technique is adopted in order to evaluate the overall behavior of the reinforced masonry accounting for

- the damage in traction of the block and the mortar,
- the damage and plasticity in compression of the block and the mortar,
- the brittle failure of the reinforcement,
- the delamination process of the FRP from the masonry.

The results obtained show the beneficial effects of the presence of the reinforcement on the overall response especially when the masonry is subjected to tension and to bending. Hence, it can be deduced that the reinforcement of the masonry should be designed in order to work in tension, i.e. when the masonry is subjected to traction or bending loading. Computations demonstrates that the delamination phenomenon affects significantly the reinforced material behavior, reducing the mechanical properties. For this reason it is very important to account for it. Furthermore, it should be noted that, when the masonry is in compression and delamination is present, the FRP could lose any loading capability, because of the instability effects of the reinforcement.

The response of the material for any loading history appears complex as it is characterized by steep softening branches and by severe snapbacks. The proposed numerical procedure, based on the arc-length

technique, is able to describe the complex behavior of the reinforced masonry, by means of an accurate choice of the control parameters. The developed analyses show good converge properties of the algorithm also in correspondence of softening and snapback branches.

The presented one-dimensional micromechanical analysis allows one to derive simple but fundamental considerations on the overall response of a reinforced masonry beam and moreover it gives some hints for developing two- or three-dimensional macromechanical models for reinforced walls.

Aim of the future development of the research is to perform micromechanical laboratory tests on the reinforced masonry and to compare the experimental results with the numerical ones which can be obtained adopting the proposed model.

Acknowledgements

The financial supports of the Italian National Research Council (CNR) and of the Ministry of University and Research (MURST) are gratefully acknowledged.

References

Anthoine, A., 1995. Derivation of the in-plane elastic characteristics of masonry through homogenization theory. International Journal of Solids and Structures 32 (2), 137–163.

Barbero, E.J., 1999. Introduction to Composite Materials Design. Taylor and Francis, London.

Bazant, Z.P., Planas, J., 1998. Fracture and Size Effects in Concrete and Other Quasibrittle Materials. CRC Press, LLC, Boca Raton, FL.

Crisfield, M.A., 1991. Non-linear Finite Element Analysis of Solids and Structures, vol. 1. Wiley, England.

El-Badry, M. (Ed.), 1996. Advanced Composite Materials in Bridges and Structures, Second International Conference, Montréal, Québec, Canada.

Gambarotta, L., Lagomarsino, S., 1997a. Damage models for the seismic response of brick masonry shear walls part I: the continuum model and its application. Earthquake Engineering and Structural Dynamics 26, 423–439.

Gambarotta, L., Lagomarsino, S., 1997b. Damage models for the seismic response of brick masonry shear walls part II: the mortar joint model and its application. Earthquake Engineering and Structural Dynamics 26, 441–462.

Giaquinta, M., Giusti, E., 1985. Researches on the equilibrium of masonry structures. Archive for Rational Mechanics and Analysis 88, 359–392.

Grimaldi, A., Luciano, R., Sacco, E., 1992. Nonlinear dynamic analysis of masonry structures via FEM. In: Glowinski, R (Ed.), Computing Methods in Applied Sciences and Engineering. Nova Science Publishers, pp. 373–382.

Heyman, J., 1966. The stone skeleton. International Journal of Solids and Structures 2, 249–279.

Kralj, B., Pande, G.N., Middleton, J., 1991. On the mechanics of frost damage to brick masonry. Computer and Structures 41 (1), 53–66.

Lemaitre, J., Chaboche, J. L., 1990. Mechanics of Solids Materials, Cambridge University Press, Cambridge, MA.

Luciano, R., Sacco, E., 1995. A micromechanical approach to the damage of the masonry material. In: Leftheris, B., Brebbia, C.A. (Eds.), Structural Studies, Repair and Maintenance of Historical Buildings STREMA 95, Computational Mechanics Publications.

Luciano, R., Sacco, E., 1996. Behavior of masonry panels reinforced with FRP composites. In: El-Badry, M. (Ed.), Proceedings of Second International Conference Advanced Composite Materials in Bridges and Structures. Montréal, Canada.

Luciano, R., Sacco, E., 1997. Homogenization technique and damage model for old masonry material. International Journal of Solids and Structures 34 (4), 3191–3208.

Luciano, R., Sacco, E., 1998. Damage of masonry panels reinforced by FRP sheets. International Journal of Solids and Structures 35 (15), 1723–1741.

Luenberger, D.G., 1973. Introduction to Linear and Nonlinear Programming. Addison-Wesley Publishing Company, Reading, MA.

Meier, U., 1987. Bridge repair with high performance composite materials. Material & Technik 4, 125–128.

Nanni, A. (Ed.), 1993. Fiber-Reinforced-Plastic Reinforcement for Concrete Structures: Properties and Applications, Elsevier, Amsterdam.

Neale, K.W., Labossière, P. (Eds.), 1992. Advanced Composite Materials in Bridges and Structures, First International Conference, Sherbrooke, Québec, Canada.

Pande, G.N., Liang, J.X., Middleton, J., 1989. Equivalent elastic moduli for brick masonry. Computers and Geotechnics 8, 243–265.
Pietruszczak, S., Niu, X., 1992. A mathematical description of macroscopic behaviour of brick masonry. Computers and Geotechnics 29 (5), 531–546.
Romano, G., Sacco, E., 1987. Convex problems in structural analysis. In: Del Piero, G., Maceri, F. (Eds.), Unilateral Problems in Structural Analysis, CISM Courses and Lectures, vol. 304. Springer, Berlin, pp. 279–297.
Schwegler, G., 1994. Masonry construction strengthened with fiber composites in seismically endangered zones. Proceedings of 10th European Conference on Earthquake Engineering, Vienna, Austria.
Simo, J.C., Hughes, T.J.R., 1998. Computational Inelasticity, Springer, Berlin.
Triantafillou, T.C., Fardis, M.N., 1993. Advanced composites for strengthening historic structures. Proceedings of the IABSE Symposium on Structural Preservation of the Architectural Heritage, Rome, Italy.
Triantafillou, T.C., Fardis, M.N., 1995. Strengthening of historic masonry structures with fiber reinforced plastic composites. In: Leftheris, B., Brebbia, C.A. (Eds.), Structural Studies, Repair and Maintenance of Historical Buildings STREMA 95. Computational Mechanics Publications.
Triantafillou, T.C., 1996. Innovative strengthening of masonry monuments with composites. Proceedings of Second International Conference Advanced Composite Materials in Bridges and Structures. Montréal, Canada.
Yim, C.S., Chopra, A.K., Penzien, J., 1990. Rocking response of rigid blocks to earthquakes. Earthquake Engineering and Structural Dynamics 88, 565–572.